ELSEVIER

Polymer 42 (2001) 2675–2684

polymer

www.elsevier.nl/locate/polymer

Isotactic polypropylene/ethylene-*co*-propylene blends: effects of composition on rheology, morphology and properties of injection moulded samples

L. D'Orazio[a,*], G. Cecchin[b]

[a]*Istituto di Ricerca e Tecnologia delle Materie Plastiche del CNR, Via Toiano, 6-80072 Arco Felice, Naples, Italy*
[b]*Montell Italia S.p.A, Ferrara, Italy*

Received 1 June 2000; received in revised form 6 July 2000; accepted 11 August 2000

Abstract

Melt rheology, phase morphology and properties of (30/70) isotactic polypropylene/ethylene-*co*-propylene (iPP/EPR) blends, containing EPR copolymer synthesised by means of a titanium based catalyst with very high stereospecific activity (EPR_{Ti}), were compared to that of (30/70) iPP/EPR blends containing EPR copolymer synthesised by using a traditional vanadium based catalyst (EPR_V). It was found that both the melts are to be classified "negative deviation blends" and that, for such a composition ratio, the EPR represents the continuous phase. Scanning electron microscopy (SEM) investigations confirmed that the iPP component segregates in spherical-shaped domains with average size lower than 1.0 μm. Such a fine degree of dispersion of the minor component in solid state is found independent of melt phase viscosity ratio and has been correlated with the interfacial tension between iPP and EPR phases. The presence of 70% of EPR copolymer dramatically interfered with the iPP crystallisation process, as strong reduction in iPP crystallinity index (X_c) values is shown by both the iPP/EPR blends. Comparatively lower X_c value is exhibited by iPP phase crystallised in presence of EPR_{Ti} copolymer. Differential scanning calorimetry (DSC) experiments revealed, in fact, that the crystallisation process of iPP phase and that of ethylenic sequences along EPR_{Ti} chains hinder each other. By small angle X-ray scattering (SAXS) it was shown that the iPP/EPR_{Ti} materials are characterised by amorphous inter-lamellar layer (L_a) considerably higher than that shown by the plain iPP and iPP phase crystallised in presence of EPR_V copolymer. This strong L_a increase was mainly ascribed to entrapping of EPR_{Ti} crystalline domains into the iPP amorphous inter-lamellar layer. Wide angle X-ray scattering (WAXS) studies demonstrated that the EPR content determines the ratio between the apparent crystal size of iPP phase grown in a direction perpendicular to the (110) crystallographic plane and the apparent crystal size of iPP phase grown in a direction perpendicular to the (040) crystallographic plane. The higher the EPR content, the higher the thickness of the iPP lamellae in the direction of the radial growth of iPP spherulites, in agreement with increased nucleation density shown by DSC results. The different modulus performance shown by the materials at room temperature was accounted for by distinguishing between effects of phase crystallinity and super-molecular structure.

Keywords: Blends; Structure; Properties

1. Introduction

Various aspects of structure–property relationships of isotactic polypropylene/ethylene-*co*-propylene (iPP/EPR) blends were extensively investigated with the focus on 80/20 composition [1–6]. It was demonstrated how the molecular structure of the single components determines, together with the crystallisation conditions of the iPP phase, the final properties of such materials. In order to investigate the effects of the EPR content on the structure–properties so far established, melt rheology, phase structure and toughening of 60/40 iPP/EPR pairs have been also studied. Results of these studies have been published recently [7]. With the aim of achieving a complete understanding of the composition effects in iPP/EPR systems, in the present paper we report on the results of investigations dealing with melt rheology, morphology and properties of 30/70 iPP/EPR blends. Two EPR samples have been synthesised ad hoc to exhibit comparable propylene content, average molecular mass and molecular mass distribution. Different catalyst systems have been used. The former EPR sample has been synthesised by means of a titanium based catalyst with very high specific activity, whereas the latter sample by

* Corresponding author. Tel.: +390-81-8534-255; fax: +390-81-8663-378.
E-mail address: dor@irtemp.na.cnr.it (L. D'Orazio).

0032-3861/01/$ - see front matter
PII: S0032-3861(00)00631-5

Table 1
Number-average molecular mass ($\bar{M}_n$), weight-average molecular mass ($\bar{M}_w$), molecular mass distribution ($\bar{M}_w/\bar{M}_n$), glass transition temperature (T_g) and apparent melting temperature (T'_m) for plain iPP and EPR copolymers together with EPR propylene content (C_3)

Sample	$\bar{M}_n \times 10^3$	$\bar{M}_w \times 10^3$	$\bar{M}_w/\bar{M}_n$	C_3 content (% wt/wt)	T_g (°C)	T'_m (°C)
iPP	78.7	509	6.5	–	7	165
EPR_{Ti}	34.8	213	6.1	38.5	− 41	122
EPR_V	30.8	199	6.5	38.5	− 43	–

using a traditional vanadium based catalyst. Effects of EPR microstructure, particularly effects of distribution of composition and sequence length of the structural units, on structure–properties relationships of 30/70 iPP/EPR injection moulded samples have been also investigated.

2. Experimental

2.1. Materials

The materials used in this study were an iPP (HS005) made by Himont and two EPR copolymers synthesised at the Himont-"Giulio Natta" Research Centre following two different procedures: the first was a synthesis process in the gas phase with a titanium based catalytic system, the second one a suspension polymerisation with a vanadium based catalytic system. The EPR copolymers so obtained have been referred to as EPR_{Ti} and EPR_V, respectively. The average molecular masses and molecular mass distribution of the starting polymers determined by means of gel permeation chromatography (GPC) in *ortho*-dichlorobenzene at the temperature of 135°C are reported in Table 1.

2.2. Blending and sample preparation

The iPP and EPR copolymers were mixed by means of a Werner mixer (Pomini PS 625) in a blending chamber with the capacity of 2.6 l. The blending process was carried out without heating, at atmospheric pressure, through agitation of the blades at 162 rpm for a time of 3.5 min. Blends with composition 30/70 (wt/wt) were prepared. After blending, the materials were injection moulded by means of an injection press (Battenfeld CD 500) at 260°C with a mould temperature of 60°C.

2.3. Techniques

Oscillatory shearing flow properties. The oscillatory shearing flow properties, namely the complex viscosity η^* (defined by $\eta^* = \eta' - i\eta''$, where η' is the dynamic viscosity or the real part of the viscosity and η'' is the imaginary part of the viscosity), the storage modulus G' (defined by $G' = \omega\eta''$, where ω is the frequency of the oscillations in radians per second) and the loss modulus G″ (defined by $G'' = \omega\eta'$) of the plain components and blends were determined at 200 and 250°C by means of a rheometrics mechanical spectrometer in the plate–plate mode with a constant strain and an angular frequency ranging between 0.01 and 100 rad s^{-1}.

Differential scanning calorimetry. The thermal behaviour of the single components and blends was analysed by means of a differential scanning calorimeter Mettler TA 3000 equipped with a control and programming unit (microprocessor Tc 10). The apparent melting temperatures (T'_m) and the crystallinity indices (X_c) of the single components and blends were determined following this procedure: the samples were heated from room temperature up to 200°C at a rate of 10°C min^{-1} and the heat evolved during the scanning process (dH/dt) was recorded as a function of temperature. The T'_m values and the apparent enthalpies of melting (ΔH^*) were obtained from the maxima and the area of the melting peaks, respectively. The crystallinity indices were calculated from the ratio between ΔH^* value and the enthalpy of melting of the 100% crystalline phase (ΔH^0) from Ref. [8].

The effect of nucleating ability of the EPR phase on the crystallisation process of iPP was investigated following this procedure: the samples were heated from room temperature up to 200°C at a rate of 10°C min^{-1} and kept at this temperature for 10 min and then they were cooled at a rate of 10°C min^{-1}.

Dynamic mechanical thermal analysis (DMTA). The loss tangent and storage modulus of samples of single components and blends were measured by means of dynamic mechanical thermal analysis (Rheometric Scientific MK III). Test data were collected in tensile mode from −100 to 100°C using a scanning rate of 1.5°C min^{-1} and a frequency of 1 Hz.

Scanning electron microscopy (SEM). iPP/EPR cryogenical fracture surfaces of injection moulded samples after coating with gold–palladium were observed by means of a scanning electron microscope (Philips XL 20).

Wide angle X-ray scattering (WAXS). WAXS studies were carried out on samples of single components and blends by means of a PW 1060/71 Philips diffractometer (Cu K_α Ni-filtered radiation) equipped with sample spinning; the high voltage was 40 kV and the tube current was 30 mA.

Small angle X-ray scattering (SAXS). SAXS studies were carried out on samples of single components and blends by means of a compact Kratky camera equipped with a Braun one-dimensional positional sensitive detector. Ni-filtered

CuK_α radiation generated from a Philips X-ray generator (PW 1730/10) operating at 40 kV and 30 mA was used. The raw scattering data were corrected for parasitic scattering, absorption and slit smearing by using Vonk's method [9]. The de-smeared intensities were then Lorentz factor corrected by multiplying by s^2 ($s = 2 \sin \theta/\lambda$) [10].

Mechanical behaviour. The tensile elastic modulus of the materials was determined by means of an Instron machine at room temperature according to ASTM D638. Notched Izod impact tests of injection moulded samples were carried out by means of a Ceast pendulum at a range of temperatures from −60 to 23°C according to ASTM D256.

3. Results and discussion

3.1. Melt rheology

Dynamic viscoelastic properties. Figs. 1 and 2 show the dependence of the logarithm of the modulus value of the complex viscosity $|\eta^*|$ upon the logarithm of the investigated frequencies for $(30/70)_{Ti}$ and $(30/70)_V$ blends, at the temperatures of 200 and 250°C, respectively. For the sake of comparison, the dependence of the logarithm of the modulus value of the complex viscosity $|\eta^*|$ upon the logarithm of the investigated frequencies at the temperatures of 200 and 250°C for $(80/20)_{Ti}$ and $(80/20)_V$ blends is also reported. As shown, 30/70 melts are pseudo-plastic (i.e. $|\eta^*|$ values decrease with increasing frequency), comparatively higher pseudo-plasticity being shown by the EPR_V containing melts. Moreover, for a given frequency, the observed decrease in $|\eta^*|$ values depends on temperature. With increasing temperature, in fact, both the melts exhibit a lower sensitivity to frequency, thus indicating that the entanglements concentration decreases with increasing temperature. Note that, irrespective of temperature, $(30/70)_{Ti}$ melts exhibit, for a given frequency, $|\eta^*|$ values lower than that shown by EPR_V containing melts. Such results indicate that iPP/EPR_{Ti} melts are characterised by lower entanglements concentration and/or that the entanglements have time to slip and relax out the stresses. The comparison between the dependence of the logarithm of the modulus value of the complex viscosity $|\eta^*|$ upon the logarithm of the investigated frequencies, shown by 30/70 and 80/20 iPP/EPR pairs, respectively, shows that with increasing copolymer content pseudo-plasticity decreases (see Figs. 1 and 2). The extent of such an effect is larger for EPR_{Ti} containing melts. The lower sensitivity to frequency exhibited by 30/70 melts could suggest that, for such a composition ratio, the EPR phase becomes the continuous phase; i.e. an inversion of phase could occur. In a previous paper [7] it was demonstrated that for a 60/40 ratio iPP still represents the continuous phase. Moreover, as also shown in Figs. 1 and 2, for both 30/70 iPP/EPR pairs, mixing results in a decrease in viscosity below the mean value of the plain components. Such a decrease becomes larger with decreasing frequency in agreement with results obtained studying 80/20 and 60/40 blends [6,7]. This effect is designated as a "negative deviation" from the following logarithm rule of mixture that applies at constant temperature and shear rate [11]:

$$\log \eta = \phi_1 \log \eta_1 + \phi_2 \log \eta_2$$

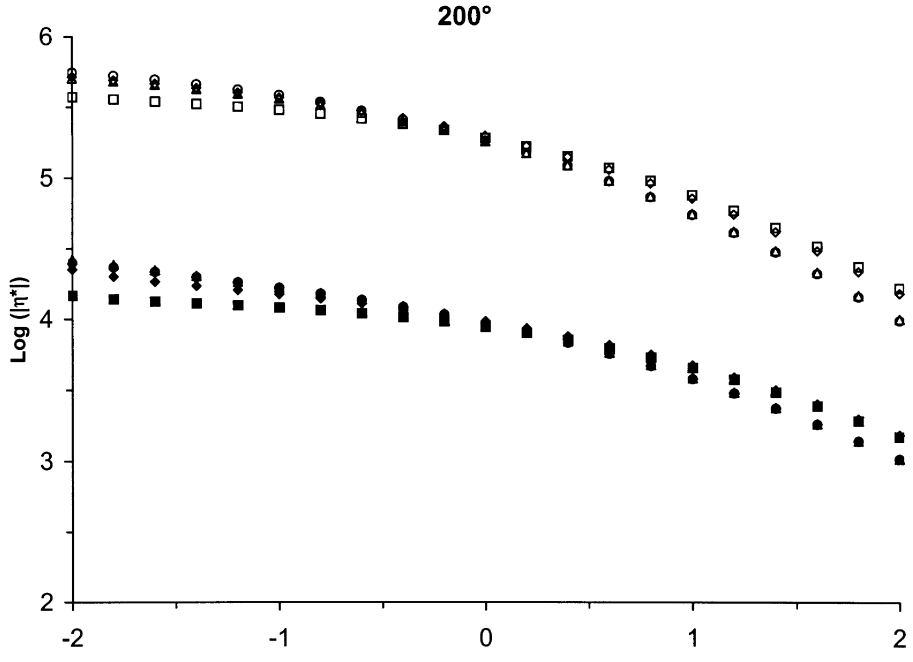

Fig. 1. Logarithm of the modulus value of the complex viscosity ($|\eta^*|$) as a function of logarithm of the frequency (ω) for iPP/EPR_{Ti} and iPP/EPR_V blends at the temperature of 200°C.

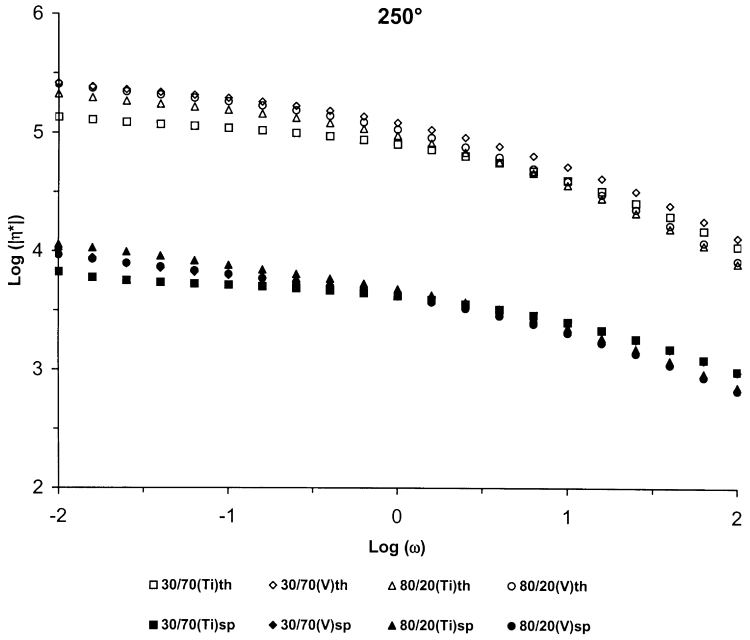

Fig. 2. Logarithm of the modulus value of the complex viscosity ($|\eta^*|$) as a function of logarithm of the frequency (ω) for iPP/EPR$_{Ti}$ and iPP/EPR$_V$ blends at the temperatures of 250°C.

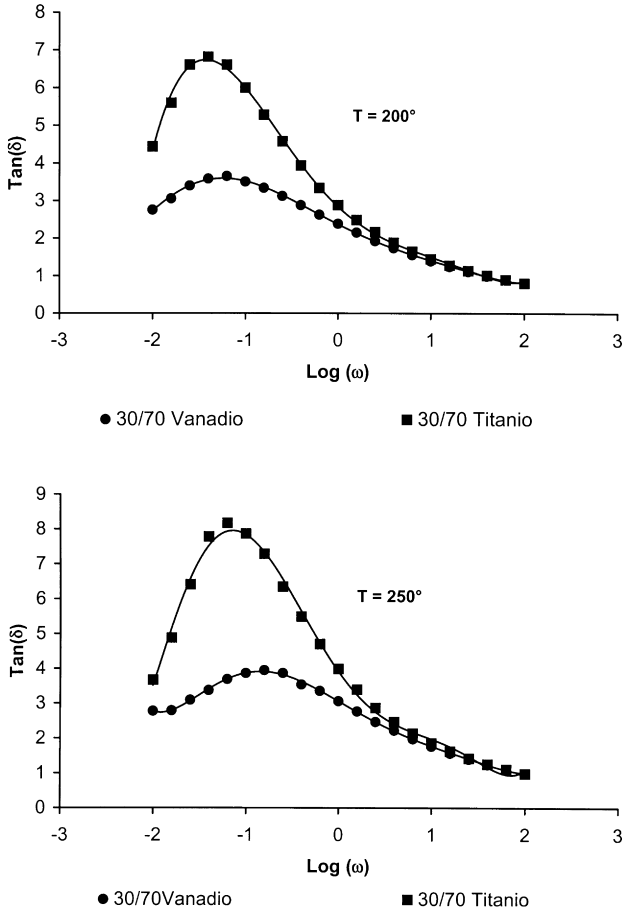

Fig. 3. tan (δ) as a function of logarithm of the frequency (ω) for iPP/EPR blends.

where η is the viscosity of the mixture, η_1 and η_2 are the viscosities of the two components measured at the same temperature, and ϕ_1 and ϕ_2 are their volume fractions. Note that, irrespective of test temperature, comparatively larger deviation is shown by the (30/70)$_{Ti}$ system (see Figs. 1 and 2). Moreover for both iPP/EPR melts, the extent of the observed negative deviation as a function of frequency increases with increasing temperature. Such a finding is to be related to the lower sensitivity shown by the melts to frequency with increasing temperature.

Fig. 3 shows the dependence of tan δ upon the logarithm of the investigated frequencies at the temperatures of 200 and 250°C for (30/70)$_{Ti}$ and (30/70)$_V$ blends. To be pointed out is that, in the first two decades of the investigated frequencies, noticeably higher elasticity is shown by the EPR$_V$ containing blends. This finding indicates that such melts are characterised by higher entanglements concentration and/or by higher time to relax out the stress and therefore by higher resistance to deformation. In other words, higher topological effects, associated with the inability of chains to pass through each other, are developed in EPR$_V$ containing melts. Taking into account that the two EPR phases have almost the same average molecular masses and molecular mass distribution, such results indicate that the different molecular interaction could be related to their different microstructure.

Determination of zero-shear viscosity and activation energy for viscous flow. Taking into account that in oscillatory measurements on polymer melts the frequency (ω) becomes analogous to shear rate (γ) [12] and assuming an approximate equivalence of η^* and apparent viscosity (η_a)

Table 2
Application of Cross equation: values of η_0, α and m for plain iPP and EPR copolymers at the temperatures of 200 and 250°C

Sample	η_0 (MPa)		α (s)		m	
	200°C	250°C	200°C	250°C	200°C	250°C
iPP	18.791	8.200	0.886	0.804	2/3	4/7
EPR_{Ti}	12.489	4.271	0.138	0.078	2/3	4/7
EPR_V	17.383	7.298	0.488	0.233	4/7	6/11

[12], the zero-shear viscosity (η_0) of both single components and blends has been calculated by using the following modified Cross–Bueche equation [13]:

$$\frac{\eta_0}{\eta_a} = 1 + (\alpha\dot{\gamma})^m$$

where η_0 is the zero-shear viscosity, α is a parameter that according to Cross should correspond to the characteristic relaxation time related to molecular mass for the linear polymer solution and m gives a measure of the shear-thinning of the melt, i.e. a measure of decrease in viscosity with increasing rate of shear. According to Iwakura and Fujimura [14] for polymer melts α is related to the size of the apparent flow unit; the reciprocal of α corresponds to the shear rate at which $\eta_a = \eta_0/2$. From the lines $1/\eta_a$ versus $\dot{\gamma}^m$ the zero-shear viscosity η_0 and α values are easily obtained from the reciprocal of the intercept and from the slope, respectively. As far as fit for such straight line plots is concerned, the R^2 values are higher than 0.99.

The m, η_0 and α values of the single components and blends at the temperatures of 200 and 250°C are reported in Tables 2 and 3, respectively. For the blends, the zero-shear viscosity values calculated assuming the additivity logarithm rule ($\eta_0{}'$) are also reported in Table 3 together with the melt phase viscosity ratio (μ) at the temperatures of 200 and 250°C. The application of the Cross equation to 30/70 iPP/EPR systems reveals that, for a given temperature, higher η_0 and α values are obtained for the melts containing EPR_V copolymer. A value of the m parameter independent of temperature is found for EPR_{Ti} containing melts, whereas a lower m value, with increasing temperature, is shown by the melts containing EPR_V copolymer (see Table 3). Moreover the η_0 values of both the blends show a negative deviation from the logarithm additivity rule, the extent of such a deviation decreasing strongly on increasing the temperature (see $\eta_0{}'$ values in Table 3). For a given temperature, larger deviation is exhibited by the EPR_V containing blends.

The blends activation energy for the viscous flow values (ΔE^*) were obtained by applying the following exponential relation accounting for the temperature dependence of the viscosity at temperatures far above the T_g or the melting point [15]:

$$\eta_0 = A \exp(\Delta E^*/RT)$$

where A is a constant characteristic of the polymer and its molecular mass, ΔE^* is the activation energy for the viscous flow, R is the gas constant and T is the temperature in Kelvin degrees. Values of ΔE^* are reported in Table 4. For sake of comparison the ΔE^* values obtained for blends containing 20 and 40% of EPR phase are also reported in Table 4. As shown, the (30/70) melts exhibit almost the same ΔE^* values, thus indicating comparable volume of the related flow elements. To be noted is that the ΔE^* values of such iPP/EPR pairs show different dependence upon composition. For EPR_{Ti} containing melts, in fact, the ΔE^* values increase with increasing copolymer content. On the other hand, the ΔE^* values calculated for iPP/EPR_V systems show a maximum for copolymer content of 40% (see Table 4).

3.2. Thermal behaviour and crystallinity

DMTA analysis shows that both $(30/70)_{Ti}$ and $(30/70)_V$ systems exhibit, as expected, two distinct glass transition temperatures (T_g) to be ascribed to EPR and iPP components, respectively. Such T_g values are reported in Table 5 and are comparable to those found for blends containing lower EPR amount (20 and 40% wt/wt) [1–7]. The differential scanning calorimetry (DSC) thermograms of samples of the $(30/70)_V$ blends show a single endothermic peak whose temperature position is characteristic of the melting of the α-form of iPP (see Table 5). Two endothermic peaks are shown by samples of the $(30/70)_{Ti}$ blends; the temperature positions of such peaks are characteristic of the melting of linear polyethylene (PE) and α-form of iPP, respectively (see Table 5). All the above results confirm that the immiscibility between iPP and EPR, both in the amorphous condensed and in the melt state, is independent of composition.

On the other hand, it is to be emphasised that the crystallinity index (X_c) of iPP phase crystallised in presence of 70% of EPR phase results decreased noticeably (see Table 5), thus indicating a strong interference of both the copolymers

Table 3
Application of Cross equation: values of η_0, α and m for iPP/EPR blends together with the zero-shear viscosity values calculated assuming log additivity (η_0') and the melt flow viscosity ratio (μ) at the temperatures of 200 and 250°C

Sample	η_0 (MPa)		α (s)		m		$\eta_0{}'$ (Pa)		μ	
	200°C	250°C	200°C	250°C	200°C	250°C	200°C	250°C	200°C	250°C
iPP/EPR_{Ti}	14.577	5.790	0.436	0.163	4/7	4/7	322793	129649	1.50	1.92
iPP/EPR_V	18.317	7.275	0.653	0.321	4/7	6/11	444893	238172	1.08	1.12

Table 4
Activation energy for the viscous flow (ΔE^*) for iPP/EPR blends

Sample	ΔE^* (J mol^{-1})
$80/20_{Ti}$	11 548
$60/40_{Ti}$	13 525
$30/70_{Ti}$	16 505
$80/20_{V}$	14 888
$60/40_{V}$	21 106
$30/70_{V}$	16 506

with the iPP crystallisation process. Note that, comparatively, the EPR_{Ti} phase interferes to a larger extent. To be considered is also that the crystallinity index of the PE phase, exhibited by the EPR_{Ti} copolymer in the presence of the iPP phase, is two times as low as that shown by the plain EPR_{Ti} copolymer. From the above it may be deduced that in iPP/EPR_{Ti} pairs the crystallisation processes of iPP and PE phases hinder each other. It is interesting to remember that for EPR_V content up to 40%, the X_c values of the iPP phase were comparable to those of plain iPP, whereas for EPR_{Ti} containing blends, such values decreased with increasing copolymer content [7]. These results indicate that the iPP crystallisation process from melts containing the EPR phase can be affected by both composition and copolymer microstructure.

The non-isothermal crystallisation exotherms of iPP/EPR blends are shown in Fig. 4. The crystallisation exotherms of plain iPP and EPR_{Ti} copolymer showed that iPP crystallises between 121 and 92°C and that EPR_{Ti} ethylenic sequences crystallise between 111 and 88°C (see Table 5). To be noted is that the non-isothermal crystallisation peaks of iPP and PE phases exhibited by iPP/EPR_{Ti} blends are convoluted together, therefore confirming a strict correlation between the two crystallisation processes. Moreover when the iPP crystallises in the presence of an EPR_{Ti} or EPR_V phase the crystallisation peak shifts to higher temperatures indicating that both the copolymers contain heterogeneous nuclei that migrate toward the iPP phase. Taking into account previous results [6,7], it can be concluded that for a given iPP/EPR pair, the observed shift to higher temperatures increases with increasing EPR content. Therefore the number of heterogeneous nuclei for the iPP volume unit, i.e. the nucleation density of the iPP phase, is composition dependent.

3.3. Phase structure

Mode and state of dispersion of the minor component. The analysis by SEM of cryogenical fracture surfaces of injection moulded bars confirms that for 30/70 iPP/EPR composition, the EPR copolymer becomes the continuous phase, the iPP representing the dispersed one. To be pointed out is that iPP mode and state of dispersion are independent of EPR molecular structure, i.e. of melt phase viscosity ratio ($\mu_1 = \eta_1/\eta_2$ where η_1 is the viscosity of the dispersed phase and η_2 that of the matrix). Comparable very fine dispersion degree of iPP domains is, in fact, achieved in both the EPR matrices, irrespective of different μ values (see Table 3). Such domains are spherically shaped with an average diameter less than 1.0 μm (see Fig. 5). It is to be pointed out that, on the contrary, a dependence of size of EPR particles dispersed in the iPP matrix upon melt phase viscosity ratio was observed for all the iPP/EPR pairs and composition investigated so far. The observed dependence was in agreement, at least qualitatively, with the trend predicted by the Taylor–Tomotika theory. According to this theory, a plot of average particle diameter ($\bar{D}_n$) versus log of melt phase viscosity ratio should show a minimum in the vicinity of $\mu = 1$ [16,17]. The different dispersion degree shown by EPR phases in the iPP matrix has been accounted for by assuming that, according to the μ value, the data points of iPP based blends can lie on both the branches of the curve reported in Fig. 6.

On the basis of the balance between the shearing force, which tends to deform the minor phase into droplets, and the interfacial tension, which tends to restore the spherical shape of the minor phase domains, the iPP minimum domain size (d_{min}), as observed in solid state samples of 30/70 iPP/EPR pairs, could be correlated with interfacial tension (σ) according to the following relation proposed by Wu [18]:

$$d_{min} = \frac{4\sigma}{\eta\dot{\gamma}}$$

where $\dot{\gamma}$ is the shear rate adopted in preparation of the

Table 5
Glass transition temperatures (T_g), apparent melting temperatures (T'_m), and crystallinity indices (X_c) for plain iPP and EPR_{Ti}, and iPP crystallised in presence of EPR_{Ti} and EPR_V copolymers; the range of non-isothermal crystallisation temperatures are also reported

Sample	T_g (°C)	T'_m (°C)	$X_{c(blend)}$ (%)	$X_{c(iPP)}$ (%)	Range of non-isothermal crystallisation temperatures (°C)
iPP	16	164	41	41	121–92
EPR_{Ti}	−41	122	6	–	111–88
		164	10	33	124–108
iPP/EPR_{Ti}	12; −37	123	2.1		108–87
iPP/EPR_V	12; −39	162	11	37	127–96

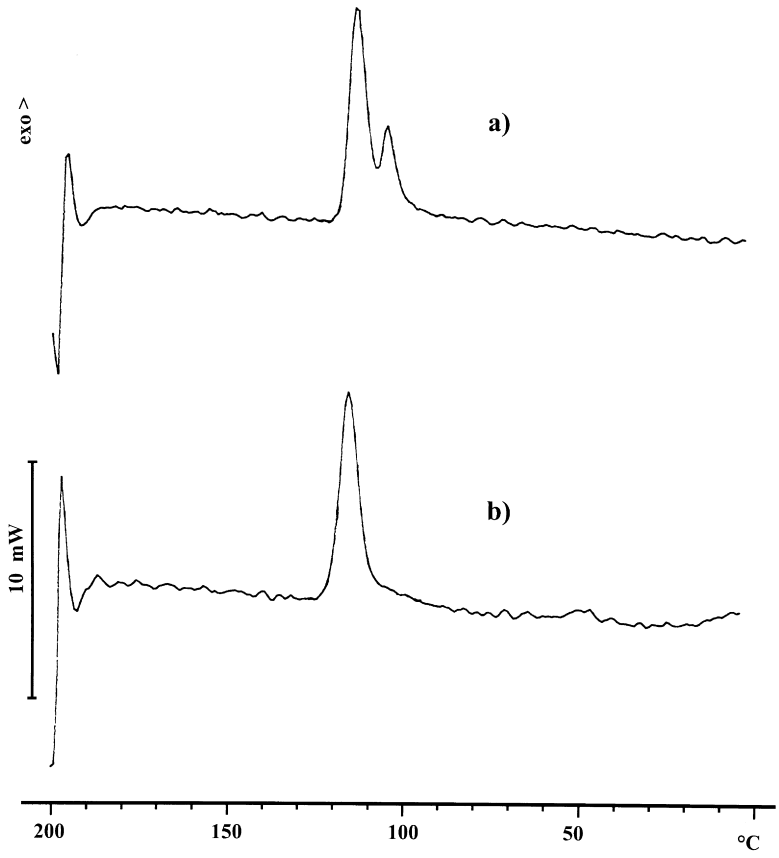

Fig. 4. Non-isothermal crystallisation curve of: (a) iPP/EPR$_{Ti}$; and (b) iPP/EPR$_V$ blends.

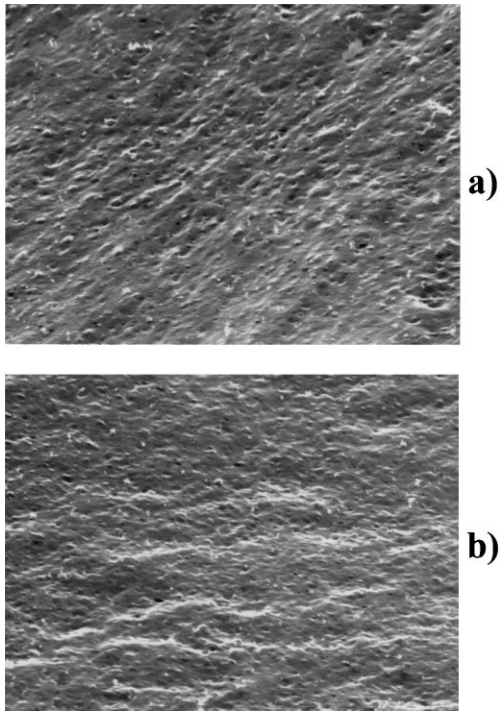

Fig. 5. SEM micrograph of cryogenical fracture surfaces of: (a) iPP/EPR$_{Ti}$; and (b) iPP/EPR$_V$ blends (3500×).

blends and η is the melt viscosity of the matrix phase. Taking into account that the same mixing process was adopted in preparation of the materials (i.e. the $\dot{\gamma}$ parameter therefore could be assumed as constant) and that the size of iPP domains is found independent of the viscosity of the EPR matrix, it can be inferred that there is comparatively lower interfacial tension between iPP and EPR$_{Ti}$ phases. In other words iPP/EPR$_V$ melts are characterised by a comparatively higher capability of restoring the spherical shape of iPP domains.

Wide angle X-ray scattering analysis. The apparent crystal size (D) of the plain iPP and iPP phase crystallised in presence of EPR copolymers in the direction perpendicular to the (110), (130) and (040) crystallographic planes has been calculated by the Sherrer equation [8]:

$$D_{hkl} = \frac{K\lambda}{\beta_0 \cos(\theta_{hkl})}$$

where β_0 is the half-width in radians of the reflection corrected for instrumental broadening and λ is the wavelength of the radiation used (1.5418 Å). The shape factor K is set equal to unity and so the size data have to be considered as relative data.

The D values calculated for plain iPP and its blends are reported in Table 6 together with the ratio between the $D_{(110)}$ values and $D_{(040)}$ values. The apparent crystal size of the iPP

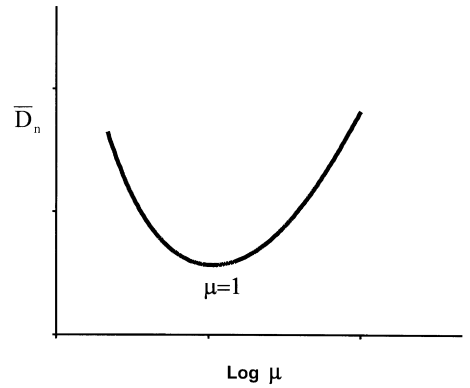

Fig. 6. Average size ($\bar{D}_n$) of dispersed particles as function of the logarithm of phase viscosity ratio (μ); trend as predicted by Taylor–Tomotika.

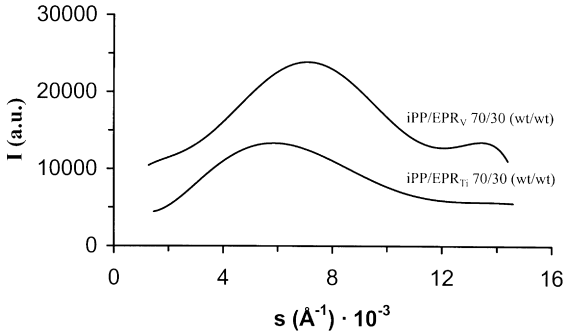

Fig. 7. De-smeared SAXS profiles for iPP/EPR blends.

phase crystallised in presence of both EPR phases is higher in the direction perpendicular to the (110) crystallographic plane and noticeably lower in the direction perpendicular to the (040) crystallographic plane than that shown by plain iPP. The $D_{(130)}$ values in the blends are found lower than that found for plain iPP, the lowest crystal size being shown by the iPP phase crystallised in the presence of the EPR_{Ti} copolymer (see Table 6). Such structural results suggest that for the iPP phase crystallised in the presence of 70% of EPR phase, the crystal growth in the directions perpendicular to the (110) and (040) crystallographic planes is larger and smaller than that shown by plain iPP. If we assume that the $D_{(110)}/D_{(040)}$ ratio represents the (D_{a^*}/D_{b^*}) ratio (i.e. the ratio between the apparent crystal size in the direction parallel to the a^* axis and the apparent crystal size in the direction parallel to the b^* axis of the iPP monoclinic unit cell), higher $D_{(110)}/D_{(040)}$ value indicates that thicker lamellae are formed in the direction of the radial growth of the iPP spherulites. The a^* axis is, in fact, the radial growth direction of the spherulite, the surface of the iPP lamellar crystal being perpendicular to the c axis. This finding is in line with higher number of nuclei for the iPP volume unit shown by DSC results. It is interesting to point out that for iPP phase crystallised in presence of 20% of EPR content, the $D_{(110)}/D_{(040)}$ ratio was found comparable to that determined for plain iPP [6], whereas, with increasing copolymer content, such a ratio increases [7]. Thus it may be concluded that when the iPP phase crystallises from iPP/EPR melts in non-isothermal conditions, the thickness of the lamellae in the directions perpendicular to the (110) and (040) crystallographic planes is composition dependent.

Table 6
Apparent crystal size (D) of plain iPP and iPP/EPR blends together with the $D_{(110)}$ and $D_{(040)}$ ratios

Sample	$D_{(110)}$ (Å)	$D_{(130)}$ (Å)	$D_{(040)}$ (Å)	$D_{(110)}/D_{(040)}$
iPP	195	220	188	1.04
iPP/EPR$_{Ti}$	214	184	77	2.78
iPP/EPR$_V$	250	198	79	3.16

Small angle X-ray scattering analysis. Typical Lorentz corrected de-smeared patterns for the iPP/EPR blends are shown in Fig. 7; note that for both the blends defined maxima are exhibited by the de-smeared SAXS profiles. Therefore from the L values, calculated by applying Bragg's law, the value of the crystalline lamellar thickness (L_c) has been calculated by using the following relation:

$$L_c = \frac{X_c L}{(\rho_c/\rho_a)(1 - X_c) + X_c}$$

where X_c is the crystallinity index and ρ_c and ρ_a are the densities of the crystalline and amorphous iPP phase, respectively [8]. Subtracting the obtained L_c value from the L value, the average thickness of the amorphous inter-lamellar layer (L_a) has been obtained. The L, L_c and L_a values so obtained are reported in Table 7 for plain iPP and its blends with EPR_{Ti} and EPR_V copolymers. As shown in Table 7, $L_{iPP/EPR}$ values are higher than the L_{iPP} value, the experimental error being ±5 Å. Thus, when iPP crystallises from (30/70) melts, the phase structure developed in such blends is characterised by an amorphous inter-lamellar layer higher than that shown by plain iPP. To be pointed out is that a very noticeable L_a increase is shown by the iPP phase crystallised in the presence of the EPR_{Ti} phase. This morphological result could be explained assuming that crystalline domains of EPR_{Ti} ethylenic sequences remain entrapped in the iPP amorphous inter-lamellar region, increasing its thickness and hindering the iPP crystal growth. What is more, by such an entrapment phenomenon also, the growth of crystalline PE domains could undergo constraint. This hypothesis agrees with DSC experiments showing that the crystallisation processes of iPP and

Table 7
Long period (L), lamellar thickness (L_c) and inter-lamellar amorphous thickness (L_a) for plain iPP and iPP/EPR blends

Sample	L (Å)	L_c (Å)	L_a (Å)
iPP	135	52	83
iPP/EPR$_{Ti}$	166	51	115
iPP/EPR$_V$	142	49	93

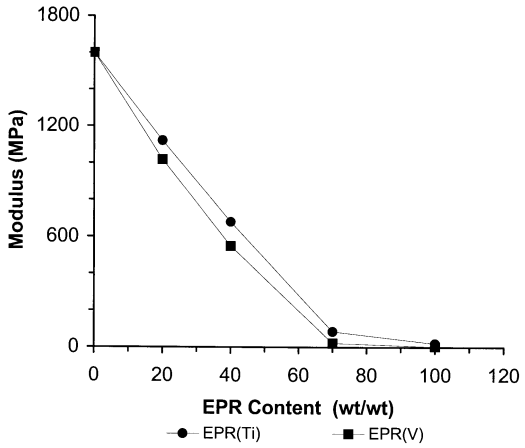

Fig. 8. Tensile elastic modulus values as a function of EPR content for iPP/EPR blends.

EPR_{Ti} PE phase are strictly correlated, hindering each other. The occurrence of a diffusion of EPR molecules with distribution of composition and length of sequences of structural units approaching that of the plain iPP into the iPP inter-lamellar amorphous layer, with formation of EPR amorphous domains more or less interconnected with the amorphous iPP phase, cannot be excluded. On the contrary, the increased L_a value shown by the iPP phase crystallised in presence of EPR_V copolymer could be accounted for by a diffusion of EPR molecules with low molecular masses into the iPP inter-lamellar amorphous layer. Finally, note that the super-reticular parameter (L_a) of iPP phase crystallised in presence of EPR_{Ti} copolymer is composition dependent, i.e. the L_a values increase with the EPR_{Ti} content [6,7].

3.4. Mechanical behaviour

The tensile elastic modulus values of plain iPP and iPP/EPR_{Ti} and iPP/EPR_V materials, for tests carried out at room temperature, are reported in Fig. 8 as a function of copolymer content (wt/wt). As shown in Fig. 8, and as is to be expected, the iPP modulus decreases with increasing EPR content. Moreover, for a given composition, lower modulus values are shown by the EPR_V based materials. The different behaviour of EPR_{Ti} and EPR_V copolymers in reducing iPP modulus is to be related to their different microstructure; i.e. to PE crystallinity shown by the EPR_{Ti} copolymer. Assuming that in a first approximation, both lamellar crystal build-up (i.e. thickening, perfection) and super-molecular organisation (i.e. inter-lamellar amorphous layer thickness and tie molecules density) contribute to determine the change in modulus as a function of crystallinity, for 30/70 iPP/EPR materials investigated the following is to be emphasised. The mode and state of dispersion of the iPP minor component into the two EPR matrices is comparable, whereas the intrinsic morphology of the iPP phase is very different. The iPP phase crystallised in presence of EPR_{Ti} copolymer is characterised by a lower crystallinity index, and, in addition, by higher inter-lamellar amorphous layer thickness. Both such effects are detrimental for modulus performance. In other words, iPP is more effective in stiffening the EPR_V matrix than the EPR_{Ti} one. The increase observed in the modulus value of these iPP/EPR materials, is, in fact, about four and seven times, respectively, the modulus value shown by plain EPR_{Ti} and EPR_V copolymers. Thus the better modulus performance exhibited by iPP/EPR_{Ti} materials is to be ascribed to combined effects related to phase morphology and structure of both the iPP minor component and the EPR_{Ti} matrix. As far as the EPR_{Ti} matrix is concerned, it is to be taken into account that the EPR_{Ti} phase crystallised in the presence of the iPP phase shows an ethylenic crystallinity lower than that exhibited by the plain copolymer. Such a reduced crystallinity induces modulus deterioration by an increase of tie molecules density, notwithstanding the beneficial effect of the ethylenic lamellar build-up. From the above it may be concluded that, even though iPP/EPR_{Ti} materials are superior to that EPR_V based on modulus performance, no real synergy can be achieved through the crystallisation process from melt of iPP and ethylenic sequences of EPR_{Ti} copolymer. Irrespective of test temperature, both the iPP/EPR materials do not break, thus no impact strength values can be measured also for temperatures lower than EPR T_g.

4. Conclusions

A study aimed at investigating effects of EPR content on melt rheology, phase morphology and properties of (30/70) iPP/EPR pairs has been performed. The following is to be remarked.

- The iPP/EPR blends investigated in this work are to be classified as "negative deviation blends".
- SEM analysis performed on injection moulded samples showed that for (30/70) composition, the copolymer represents the continuous phase. Fine dispersion degree of iPP spherical-shaped domains is achieved in both the iPP/EPR pairs (average size lower than 1.0 μm), with no dependence of particle size of minor component upon melt phase viscosity ratio (i.e. upon EPR molecular structure). Thus it has been inferred that there is comparatively lower interfacial tension between iPP and EPR_{Ti} phase.
- The EPR microstructure strongly affects both the crystallisation process of the iPP phase and the inner structure of the iPP spherulites (i.e. thickness of the amorphous inter-lamellar layer (L_a)).
- WAXS studies revealed that the EPR content determines the ratio between the apparent crystal size of the iPP phase in the direction perpendicular to the (110) crystallographic plane and the apparent crystal size of the iPP phase in the direction perpendicular to the (040) crystallographic plane.

- At room temperature better tensile elastic behaviour is shown by EPR_{Ti} based materials, even though it has been shown that the iPP phase is more effective in stiffening the EPR_V matrix. In other words, for an iPP/EPR_{Ti} pair no real synergy with respect to modulus performance can be developed through the crystallisation process from the melt of iPP and ethylenic sequences of copolymer.

References

[1] D'Orazio L, Mancarella C, Martuscelli E. Polymer 1991;32:1186.
[2] D'Orazio L, Mancarella C, Martuscelli E, Sticotti G. J Mater Sci 1991;26:4033.
[3] D'Orazio L, Mancarella C, Martuscelli E, Sticotti G. Polymer 1993;34:3671.
[4] D'Orazio L, Mancarella C, Martuscelli E, Sticotti G. J Appl Polym Sci 1994;53:387.
[5] D'Orazio L, Mancarella C, Martuscelli E, Sticotti G. Advanced routes for polymer toughening. Amsterdam: Elsevier, 1996 (chap. 5).
[6] D'Orazio L, Mancarella C, Martuscelli E, Sticotti G. J Appl Polym Sci 1999;72:701.
[7] D'Orazio L, Mancarella C, Martuscelli E. Polymer 1999;40:2745.
[8] Brandup S, Immergut EM. Polymer handbook, vol. 5. New York: Interscience, 1975 (p. 16–28).
[9] Vonk CG. J Appl Crystallogr 1975;8:340.
[10] Alexander LE. X-ray diffraction in polymer science. New York: Wiley, 1969.
[11] Utraki CA, Kamal MR. Polym Engng Sci 1982;22:96.
[12] Ferry JD. Viscoelastic properties of polymers. 2nd ed. New York: Wiley, 1970.
[13] Cross MM. J Appl Polym Sci 1969;13:765.
[14] Iwakura K, Fujimura T. J Appl Polym Sci 1975;19:1427.
[15] Van Krevelen DW. Properties of polymers. New York: Elsevier, 1976.
[16] Taylor GI. Proc R Soc Lond (A) 1934;146:501.
[17] Tomotika S. Proc R Soc Lond (A) 1936;153:322.
[18] Wu S. Polym Engng Sci 1987;27:335.